Available online at www.sciencedirect.com
SCIENCE DIRECT
Journal of the European Ceramic Society 25 (2005) 1447–1453
www.elsevier.com/locate/jeurceramsoc

Raman/Cr^{3+} fluorescence mapping of a melt-grown $Al_2O_3/GdAlO_3$ eutectic

G. Gouadec [a,*], Ph. Colomban [a], N. Piquet [b,c], M.F. Trichet [b], L. Mazerolles [b]

[a] *LADIR, UMR 7075, CNRS—Université P. et M. Curie, 2 rue Henri Dunant, 94320 Thiais, France*
[b] *CECM, UPR 2801, CNRS, 15 rue Georges Urbain, 94407 Vitry-sur-Seine, France*
[c] *ONERA, DMSC, BP 72, 92322 Châtillon, France*

Available online 15 February 2005

Abstract

The paper reports on the Raman/fluorescence study of a melt-grown $Al_2O_3/GdAlO_3$ eutectic composite. Raman bands from the α-alumina and gadolinium perovskite phases identified by X-ray diffraction were systematically observed together in the optically visible domains, even when the latter were much larger than the Raman probe. This suggests a more complex interlocking pattern than appearing on SEM or optical microscopy images. The polarization of alumina and $GdAlO_3$ Raman bands evidenced the preferential orientation of Al_2O_3 phase with respect to the sample growth direction, in agreement with TEM results. In addition, the position of chromium impurity fluorescence bands was used to map the residual stress in alumina phase. It is a compression in the 200–300 MPa range.

Keywords: Stress mapping; Electron microscopy; Spectroscopy; Al_2O_3; Perovskites

1. Introduction

Directionally solidified eutectic ceramics are refractory materials that could be used for high-temperature structural applications (blades in the airspace and power generation industries) and in electrical, optical, piezoelectric or ferromagnetic devices.[1–3] Like particulate composites, these "natural" composites exhibit isotropic properties.[4,5] Moreover, their interlocked microstructure results in a very high creep resistance[6,7] which, in conjunction with their intrinsic resistance to oxidation, makes them an interesting alternative to traditional fibre-reinforced composites. Eutectic compositions in several Al_2O_3–Ln_2O_3 systems are studied at CECM, associating alumina with either a perovskite (Ln = Gd, Eu) or a garnet (Ln = Dy, Er, Yb) structure.

Nakagawa and co-workers studied $Al_2O_3/GdAlO_3$ eutectic samples[2] and the purpose of this paper is to use Raman analysis for composition and structural investigation of similar material prepared at CECM. The use of Cr^{3+} fluorescence stress sensitivity will also allow for residual stress assessment, as was already done in polycrystalline alumina,[8] epoxy-embedded alumina fibers[9] and alumina/zirconia composites of eutectic[3,10] or non-eutectic[11–13] compositions.

2. Experimental

2.1. Synthesis and characterization of the samples

Rods of oriented eutectics were grown by floating-zone translation using an arc image furnace operating with a 6-kW xenon lamp as radiation source. The starting material was prepared by mixing 99.9% pure polycrystalline powders of Al_2O_3 (Baikowski Chimie, France, grain size ≤1 μm) and Gd_2O_3 (Rhodia, formerly Rhône-Poulenc Chimie, France, grain size ≤2 μm). The proportions were 48.5 wt.% Al_2O_3 with 51.5 wt.% Gd_2O_3, which corresponds to the eutectic composition 77 mol% Al_2O_3–23 mol% Gd_2O_3.[14] Cylinders were isostatically pressed at 150 MPa, which was followed by 10 h sintering at 1775 K. Two cylinders (length: 4 cm; diameter: 6 mm) were then set in the arc image furnace, as

* Corresponding author. Fax: +33 1 49 78 13 18.
E-mail address: gouadec@glvt-cnrs.fr (G. Gouadec).

0955-2219/$ – see front matter © 2005 Elsevier Ltd. All rights reserved.
doi:10.1016/j.jeurceramsoc.2005.01.024

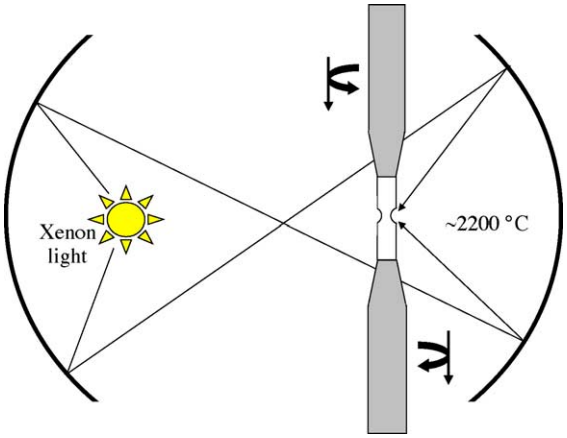

Fig. 1. Schematic of the arc image furnace used to grow directionally solidified Al_2O_3/$GdAlO_3$ eutectics.

shown in Fig. 1. After a liquid droplet was obtained at the focal point, indicating the eutectic temperature of 1976 K had been reached, the whole set-up was driven down at a constant speed of either 2 or 5 mm h^{-1}. This was done in air with a high thermal gradient of 6.10^4 K m^{-1}. As-prepared rods had a diameter of about 8 mm with a length between 3 and 5 cm, depending on the growth rate. These rods were eventually cut in either longitudinal or cross-sectional directions and their surfaces were polished to the micron using diamond paste.

X-ray powder patterns recorded with a PW 1830 Philips diffractometer (using the $\lambda = 0.17889$ nm Kα radiation of cobalt) allowed for identification of the different phases and calculation of the lattice parameters. Some X-ray diagrams were also recorded on surfaces perpendicular to the growth direction (transverse section). Phase orientation was obtained from Transmission Electron Microscopy (TEM) diffraction patterns. These were recorded with a Jeol2000EX electron microscope (operating at 200 kV) on thinned foils of transverse section prepared by mechanical polishing and ion-milling. A Au–Pd-coated sample was also observed with a Leo1530 (Leo, Germany) Scanning Electron Microscope (SEM) equipped with a Princeton Gamma Tech (USA) EDX accessory.

3. Raman equipment

All Raman spectra were recorded using a "XY" spectrograph (Dilor, France) equipped with a double monochromator as a filter and a back-illuminated liquid nitrogen-cooled 2000 × 800 pixels CCD detector (Spex, a division of the Jobin-Yvon Company, France). The laser excitation was focused on the sample through a microscope objective and the backscattered light analysed ("microRaman spectroscopy"). We used the $\lambda = 514.5$ nm line of a "Innova 70" Argon–Krypton laser source (Coherent, USA) and the laser power (see figure legends) was measured under the microscope objective using a "PD200" photodiode detector (Ophir, USA).

4. Results and discussion

4.1. X-ray analysis/electron microscopy

X-ray powder analysis revealed the presence in our samples of trigonal Al_2O_3 (α-alumina, $a = 0.47585$ nm, $c = 1.2973$ nm) and orthorhombic $GdAlO_3$ perovskite (GAP, $a = 0.52507$ nm, $b = 0.53007$ nm, $c = 0.7449$ nm). Because of thermal gradients, controlling the microstructure of directionally solidified eutectic materials is difficult and heterogeneous features are obviously present in the outer region of our samples cross section (Fig. 2a and b). We shall focus on the central region where SEM micrographs (Fig. 2c) resemble those Nakagawa et al. got from three-dimensionally and continuously interlocking phases.[2] In this region, our surface X-ray diagrams show $[0\,1\,\bar{1}\,0]$ is Al_2O_3 preferential growth direction. Besides, electron diffraction patterns obtained with the selected area aperture centred on Al_2O_3–GAP interfaces give $[1\,\bar{1}\,0]$ $GdAlO_3$ // $[0\,1\,\bar{1}\,0]$ Al_2O_3 as the predominant relative orientation (Fig. 3).

4.2. The average Raman spectrum

Fig. 4a shows an average spectrum for the sample melt-grown at 5 mm h^{-1} speed. Fig. 4b shows Raman bands are the same in the sample melt-grown at 2 mm h^{-1}. α-Alumina bands[15] are marked in Fig. 4a and Table 1 gives the 21 other modes that we observed. These additional bands presumably come from GAP phase. 24 Raman-active modes are expected in orthorhombic perovskites[16] and Chopelas[17] mentioned detecting 22 of them in GAP samples but these authors did not disclose the corresponding wavenumbers.

In a "molecular" description of material vibrations, wavenumbers below 300 cm^{-1} typically correspond to R′/T′ modes, wavenumbers between 300 and 450 cm^{-1} to bend-

Table 1
Raman wavenumbers in GAP phase (cm^{-1}): **very intense**/**intense**/(uncertain)

59	**R'/T' (Gd cation)**
93.5	
146	
172	
215	
223	
233	
(281)	
315	**δ AlO_6**
366	
384	
399	
405	
(440)	
470	
522	**ν AlO_6**
534	
(630)	
(670)	
(713)	
(720)	

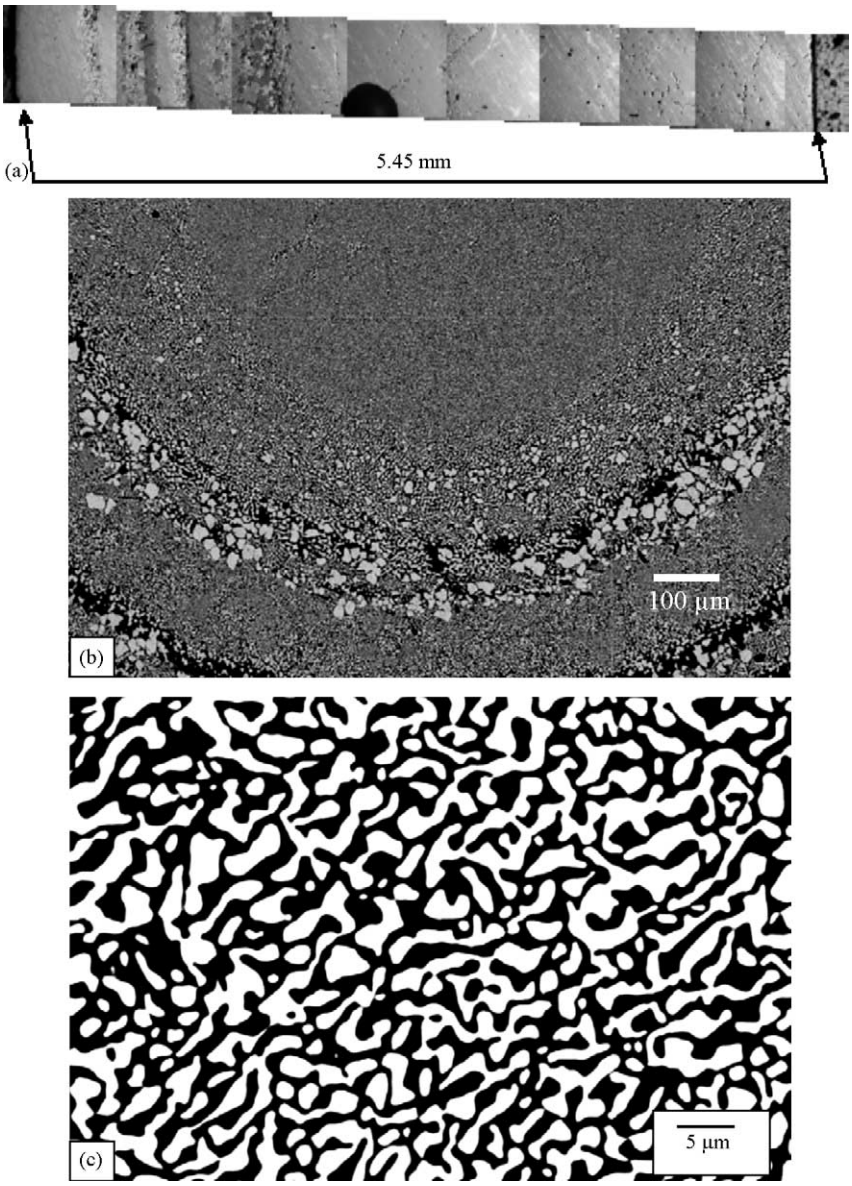

Fig. 2. Cross section views of the $Al_2O_3/GdAlO_3$ rod melt-grown at 2 mm h^{-1} speed: (a) radial optical micrograph (rod centre is to the right); (b) SEM micrograph (bar = 100 μm); (c) "BSE" (backscattered electrons) SEM micrograph taken in the central region of the rod (bar = 5 μm).

ing modes and wavenumbers above 450 cm^{-1} to stretching modes. In oxides other than GAP, cationic disorder and oxygen vacancies were shown to widen R′/T′[18] and stretching[19] modes, respectively. The transposition of these trends to the relatively narrow peaks of GAP phase suggests a good level of ordering with, possibly, some "chain-like" anisotropy ("strong" intensity of R′-like modes[19]). Yet, further study on our specific material is needed to ascertain these conjectures.

4.3. Phase distribution

All the "black", "grey" and "white" regions visible in the optical micrographs of Figs. 2a, 5a and 6 exhibited a combined Al_2O_3/GAP spectrum (Fig. 5b), even when they had a much larger extension than the lateral resolution of the spot (∼1 μm[20]). If these phases' thickness was also greater than laser penetration, which is likely given that the depth of field of our ×100 objective (numerical aperture = 0.80) is 0.833 μm only,[21] then these regions must be intricate mixtures of alumina and GAP in various proportions. As a matter of fact, the Raman cross section of GAP can be expected to be much stronger than that of alumina (Gd^{3+} is a heavy cation) and the darker regions in Fig. 5a could be almost "pure" Al_2O_3 (very weak GAP contribution).

4.4. Phase orientation

The electric field radiated in case of Raman scattering is proportional to the polarisability change occurring when

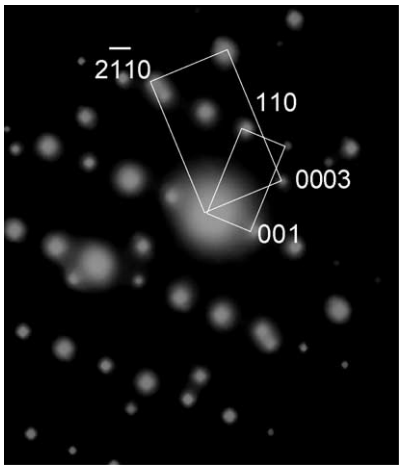

Fig. 3. Electron diffraction pattern relative to the $[0\,1\,\bar{1}\,0]$ Al_2O_3 // $[1\,\bar{1}\,0]$ $GdAlO_3$ orientation. The large and small rectangles correspond to alumina and $GdAlO_3$ lattices, respectively.

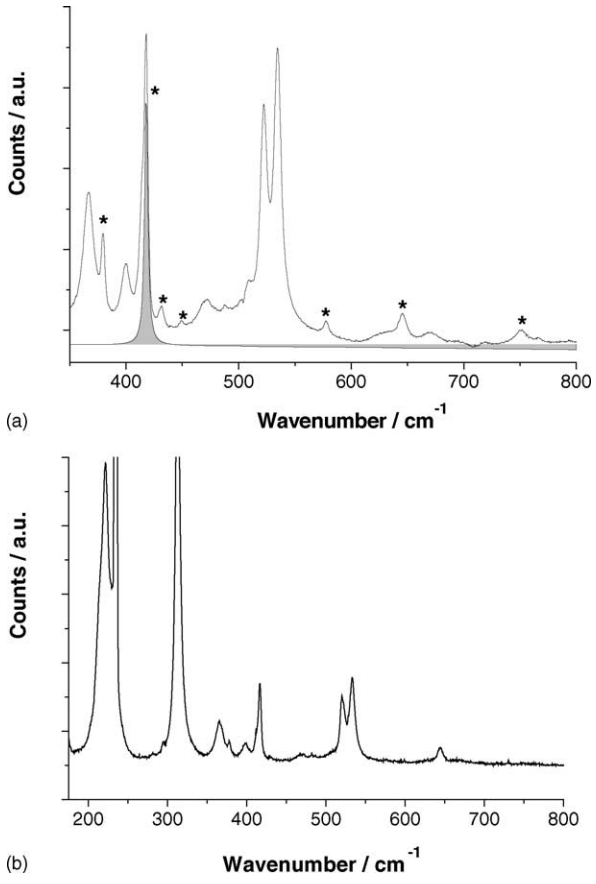

Fig. 4. (a) Raman signal recorded on the polished cross-section of the sample melt-grown at 5 mm h^{-1}. The spectrum is an average from a 22 × 22 array of 120-s -spectra recorded over a 10 μm × 10 μm square region (power: 6.6 mW; microscope objective: ×100lf). Stars indicate α-alumina signature. The specific contribution to the 417 cm^{-1} peak is highlighted. (b) Raman spectrum recorded on the polished cross-section of the sample melt-grown at 2 mm h^{-1} (spot $\phi \sim 1$ μm, power: 1.65 mW, microscope objective: ×100 lf, $t = 3600$ s).

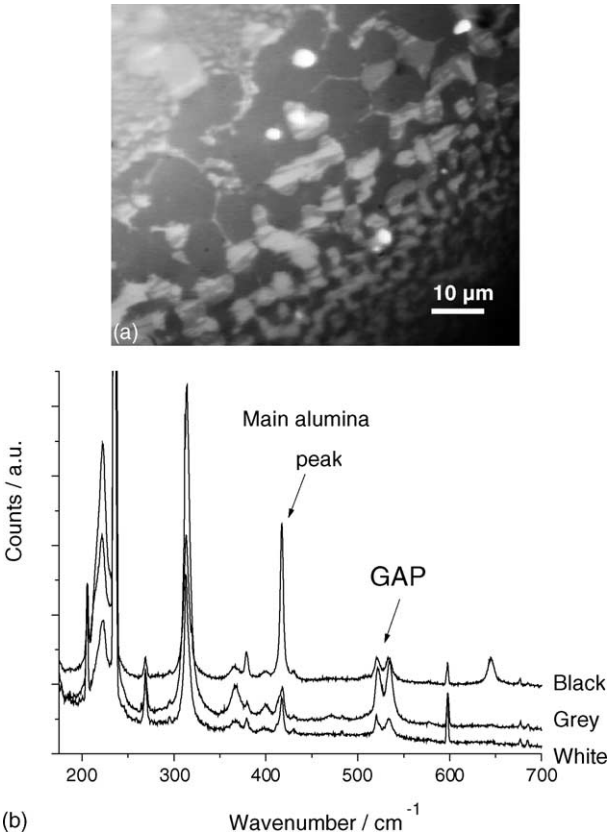

Fig. 5. (a) optical micrograph of the cross section of the Al_2O_3/GAP sample melt-grown at 2 mm h^{-1} solidification rate; (b) Raman spectra recorded in the centre of ∼10 μm diameter regions (objective: ×100 lf/spot $\phi \sim 1$ μm, $P = 2.83$ mW, 1200 s per spectrum). Labels indicate the colour of each probed region as it appears in (a).

laser light interacts with atomic vibrations. This tensorial dependency makes Raman intensity a function of the relative sample to laser orientation[15] and can be used to observe crystallographic orientations.

Fig. 6 shows optically identifiable domains were oriented along "preferential" directions in our samples. Raman spectra were recorded both in cross-section and longitudinal views with the laser excitation polarized either parallel ($\theta = 0°$) or perpendicular ($\theta = 90°$) to these directions (Table 2). The average spectra are shown in Fig. 7. First, there is no obvious balancing of band intensities in GAP and we cannot conclude on any preferential orientation of this phase. As for α-alumina, its 577, 647 and 741 cm^{-1} modes behave dif-

Table 2
Spectra recorded on cross-section and longitudinal views for an angle θ between the preferential direction and incident electric field

Sample configuration	θ angle (°)	Number of spectra	Power/time per spectrum
Cross section	0	81	6.4 mW/600 s
	90	90	6.4 mW/600 s
Longitudinal	0	50	6.0 mW/900 s
	90	9	9.2 mW/600 s

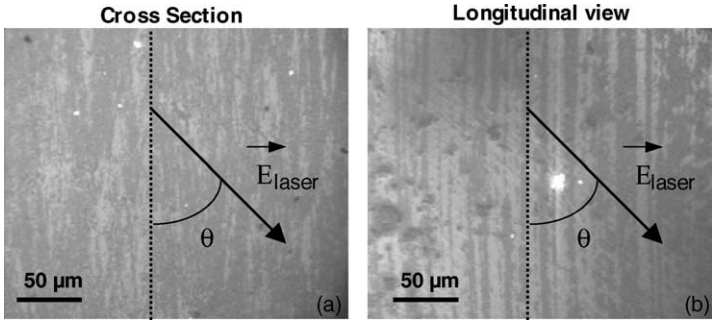

Fig. 6. Optical micrographs of the cross-section (a) and the "longitudinal" view (b) of the Al_2O_3/GAP sample melt-grown at 2 mm h^{-1} solidification rate. θ is the angle between the laser polarization and the main domains orientation (see Raman spectra of Fig. 7).

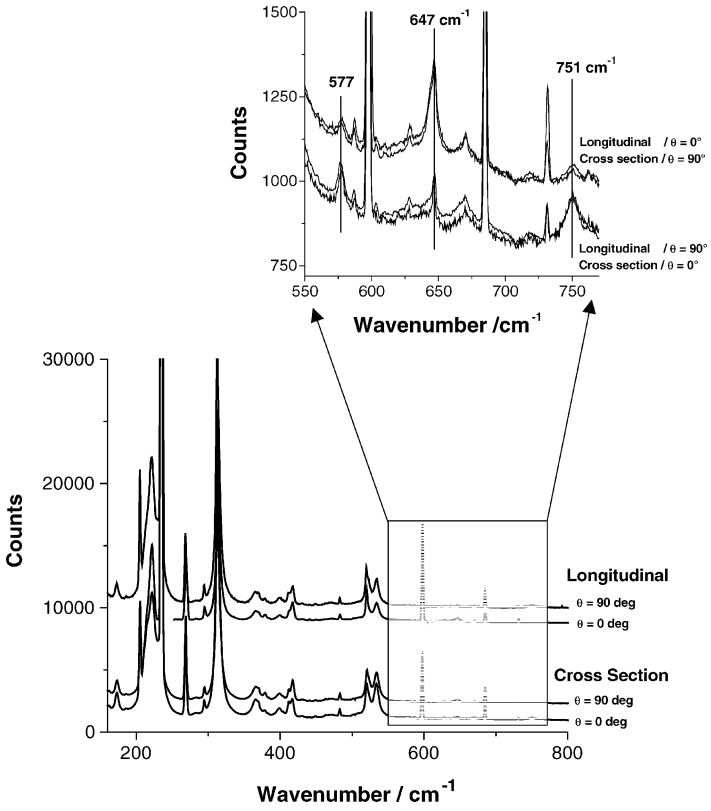

Fig. 7. Orientation dependence of Raman signal (see Fig. 6). Each spectrum is the average of 9–90 spectra (listed in Table 2). The 550–775 cm^{-1} region is magnified to show α-alumina bands at 577, 647 and 751 cm^{-1}.

ferently as a function of θ angle, both in cross section and longitudinal probing, which indicates preferential orientation (see Table 3). Further work will involve systematic mapping, alumina bands intensity ratio giving a direct image of crystallographic orientation throughout the material.

Table 3
Symmetry of selected alumina modes (D_{3d} group)

Wavenumber (cm^{-1})	Mode symmetry	Raman polarization
577 751	E_g	$(\alpha_{xx} - \alpha_{yy}, \alpha_{xy})$; $(\alpha_{xz}, \alpha_{yz})$
647	A_{1g}	$(\alpha_{xx} + \alpha_{yy}, \alpha_{zz})$

4.5. Residual stress assessment

The stress-dependant shift of the so-called R_1 and R_2 fluorescence lines of chromium impurities is a widely reported way of measuring stress in alumina.[3,8–13,22] Yet, Raman spectrometers not being perfectly stable, accurate stress determination requires that these lines be pointed with respect to an absolute reference. This is done in Fig. 8 through the value of Δ_{wav}, which is defined using the 7032.4134 Å (14219.87 cm^{-1}) emission line of a neon lamp[23] as the reference. Fig. 9 shows Δ_{wav} measured in the precursor mixture of Al_2O_3 and Gd_2O_3 powders is very sensitive to laser power. Even at very low values, not all input energy can dissipate (air is a very poor heat conductor) and temperature starts rising at the laser impact. The subsequent disturbance of the electronic energies results in a downward shift,[24] which we fitted as follows:

$$\Delta_{way}\,(cm^{-1}) = 183.27 - 0.0935 \times \mathrm{Ln}\,P\,(mW) \qquad (1)$$

Taking 183.27 cm^{-1} as the heating-corrected stress free value for Δ_{wav} and knowing that R_1 shifts under hydrostatic stress by an amount of 8.05 cm^{-1} GPa^{-1},[25] then alumina

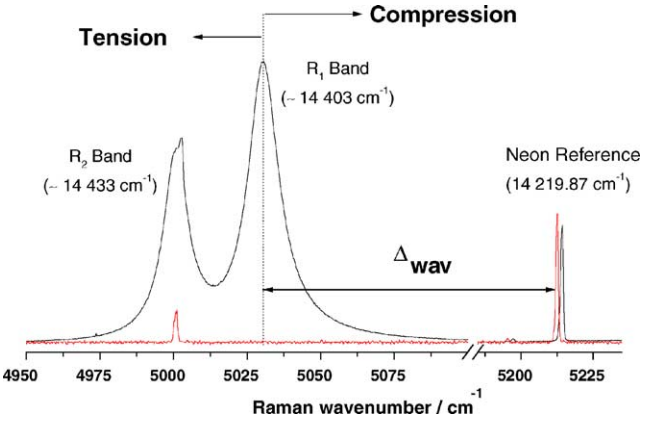

Fig. 8. Neon emission spectra, with and without Cr^{3+} fluorescence spectrum (R_1 and R_2 ruby lines). The apparent shift of the 14219 cm^{-1} reference line shows spectrometer instability. Note the difference between the absolute wavenumbers (numbers in brackets) and Raman wavenumbers, which actually indicate the shift with respect to the laser wavenumber.

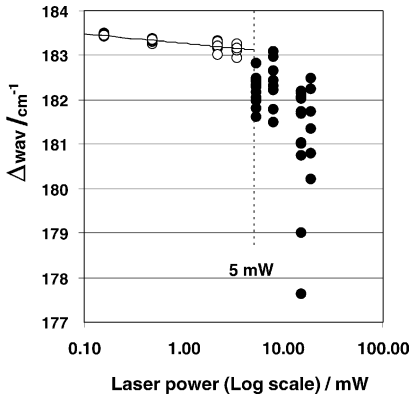

Fig. 9. Effect of laser power on Δ_{wav} (see Fig. 8) for the precursor mixture (pm) of Al_2O_3 and Gd_2O_3 powders. Data fitting for $P < 5$ mW (37 points) yields: Δ_{way}^{pm} (cm^{-1}) = 183.27 − 0.0935 × Ln P (mW).

residual stress in our Al_2O_3/GAP eutectic is given by:

$$\sigma\,(\text{GPa}) = \frac{\Delta_{way}\,(\text{cm}^{-1}) + 0.0935 \times \text{Ln}\,P\,(\text{mW}) - 183.27}{8.05} \quad (2)$$

Fig. 10 shows two examples of stress mappings based on Eq. (2). Note this equation was established assuming that:

(i) eutectic composites have the same thermal conductivity as the precursor powder (the 0.0935 × Ln(P) correction comes from Eq. (1)). It might not be the case but (0.0935 × Ln P)/8.05 only represents 12 and 6 MPa in Fig. 10a and b, respectively. This is relatively low when compared with a residual compression >200 MPa.

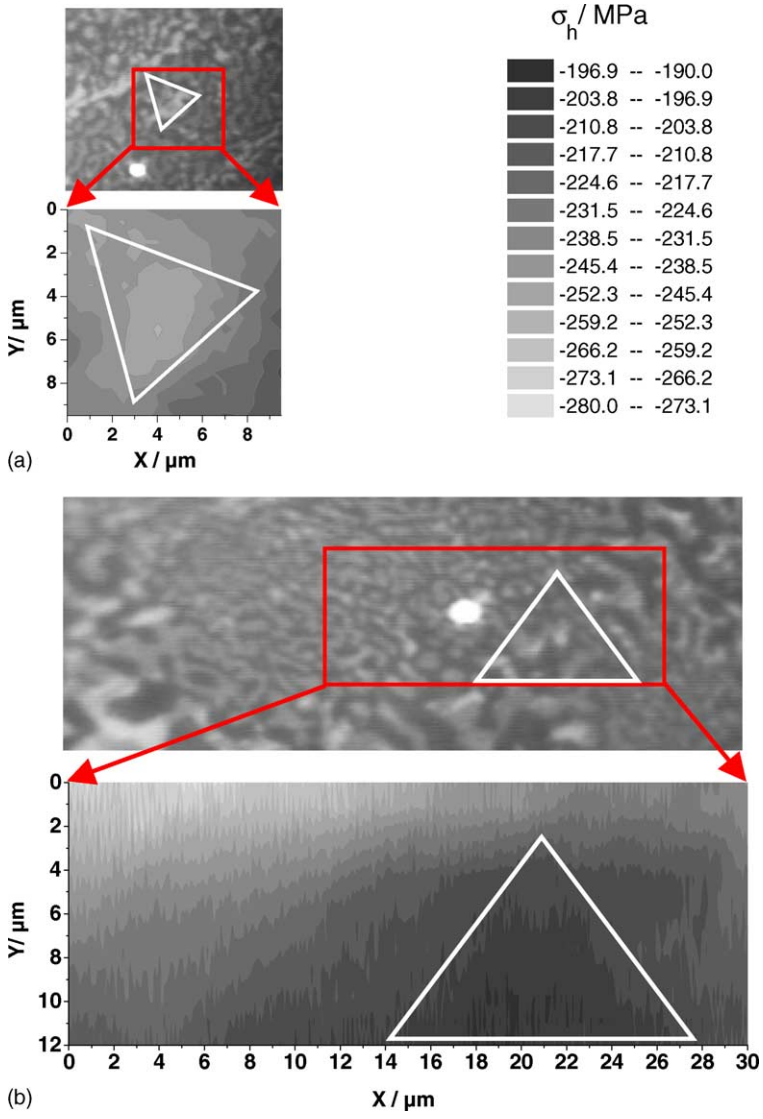

Fig. 10. Residual stress mappings based on application of Eq. (2) to the Al_2O_3/GAP sample melt-grown at 2 mm h^{-1} solidification rate. (a) 20-s Raman spectra were recorded over the 9.5 µm × 9.5 µm framed region (20 × 20 spectra; objective: ×100 lf; P = 2.9 mW); (b) 10-s Raman spectra were recorded over the 30 µm × 12 µm framed region (300 × 12 spectra; objective: ×100 lf; P = 1.65 mW). White triangles were added to highlight similarities between the microstructure and stress gradients.

(ii) the residual stress is hydrostatic. As a matter of fact, R_2 line would have been less sensitive to stress anisotropy[8,10,25] but a small neon line emitted in its spectral domain forced us to work with R_1 as the stress probe.

The position of alumina Raman bands would be an alternative way of measuring residual stress.[26–28] It is much longer to get a useful signal but gives access to stress in the different directions of the crystals (bands are polarized). Note also that Cr^{3+} must be present in the GAP phase but we could not detect a nice enough fluorescence signal to use it for stress measurement, as did Jovanić and Andreeta in Cr^{3+}-doped $GdAlO_3$.[29]

5. Summary—perspectives

X-ray diffraction evidenced α-alumina and gadolinium aluminium perovskite are the constitutive phases of a melt-grown $Al_2O_3/GdAlO_3$ eutectic ceramic. TEM results showed alumina is an extending monocrystal whereas GAP phase tends to orientate along interfaces only.

Distinct domains were identified through optical and electronic microscopies, the Raman spectrum of which always combined Al_2O_3 and $GdAlO_3$ signal. This suggests fine micro-/nano-interlocking in each domain. The bands polarization confirmed alumina is oriented parallel to the crystal growth direction and must therefore strongly influence mechanical properties.

Lastly, the shift of Ruby fluorescence lines with respect to their stress-free position indicated alumina is subjected to a residual compressive stress in the 200–300 MPa range.

References

1. Stubican, V. S. and Bradt, R. C., Eutectic solidification in ceramic systems. *Annu. Rev. Mater. Sci.*, 1981, **11**, 267–297.
2. Nakagawa, N., Waku, Y. and Wakamoto, T., A new unidirectional solidified ceramic eutectic with high strength at high temperatures. *Mater. Manufact. Process.*, 2000, **15**, 709–725.
3. Pardo, J. A., Merino, R. I., Orera, V. M., Peña, J. I., González, C., Pastor, J. Y. *et al.*, Piezospectroscopic study of residual stresses in Al_2O_3–ZrO_2 directionally solidified eutectics. *J. Am. Ceram. Soc.*, 2000, **83**, 2745–2752.
4. Chawla, K. K., *Composite Materials Science and Engineering* (*2nd ed.*). Springer-Verlag, New York, 1998.
5. Michel, D., Mazerolles, L., Bruneton, E., Portier, R. and Colomban, Ph., Interfaces and microstructures in ceramic–ceramic composites. *Ann. Chim. Fr.*, 1991, **16**, 487–496.
6. Argon, A., Yi, J. and Sayir, A., Creep resistance of directionally solidified ceramic eutectics of Al_2O_3/c-ZrO_2 with sub-micron columnar morphologies. *Mater. Sci. Eng.*, 2001, **A319–321**, 838–842.
7. Sayir, A. and Farmer, S. C., The effect of the microstructure on mechanical properties of directionally solidified Al_2O_3–$ZrO_2(Y_2O_3)$ eutectic. *Acta Mater.*, 2000, **48**, 4691–4697.
8. Pezzotti, G., In situ study of fracture mechanisms in advanced ceramics using fluorescence and Raman microprobe spectroscopy. *J. Raman Spectr.*, 1999, **30**, 867–875.
9. Mahiou, H., Beakou, A. and Young, R. J., Investigation into stress transfer characteristics in alumina-fibre/epoxy model composites through the use of fluorescence spectroscopy. *J. Mater. Sci.*, 1999, **34**, 6069–6080.
10. Harlan, N. R., Merino, R. I., Peña, J. I., Larrea, A., Orera, V., Gonzalez, C. *et al.*, Phase distribution and residual stresses in melt-grown Al_2O_3–$ZrO_2(Y_2O_3)$ eutectics. *J. Am. Ceram. Soc.*, 2002, **85**, 2025–2032.
11. Pezzotti, G., Sergo, V., Sbaizero, O., Muraki, N., Meriani, S. and Nishida, T., Strengthening contribution arising from residual stresses in Al_2O_3/ZrO_2 composites: a piezo-spectroscopy investigation. *J. Eur. Ceram. Soc.*, 1999, **19**, 247–253.
12. Merlani, E., Schmid, C. and Sergo, V., Residual stresses in alumina/zirconia composites: effect of cooling rate and grain size. *J. Am. Ceram. Soc.*, 2001, **84**, 2962–2968.
13. Sergo, V., Pezzotti, G., Sbaizero, O. and Nishida, T., Grain size influence on residual stresses in alumina/zirconia composites. *Acta Mater.*, 1998, **46**, 1701–1710.
14. Levin, E. M., Robbins, C. R. and McMurdie, H. F., *Phase Diagrams for Ceramists*. The American Ceramic Society, Columbus, OH, 1964.
15. Porto, S. P. S. and Krishnan, R. S., Raman effect of corundum. *J. Chem. Phys.*, 1967, **47**, 1009–1012.
16. Martín-Carrón, L. and De Andrés, A., Melting of the cooperative Jahn–Teller distortion in $LaMnO_3$ single crystal studied by Raman spectroscopy. *Eur. Phys. J.*, 2001, **B22**, 11–16.
17. Chopelas, A., Thermal expansivity of lower mantle phases MgO and $MgSiO_3$ perovskite at high pressure derived from vibrational spectroscopy. *Phys. Earth Plan. Inter.*, 1996, **98**, 3–15.
18. Meng, J. F., Katiyar, R. S. and Zou, G. T., Grain size effect on ferroelectric phase transition in $Pb_{1-x}Ba_xTiO_3$ ceramics. *J. Phys. Chem. Solids*, 1998, **59**, 1161–1167.
19. Colomban, Ph., Romain, F., Neiman, A. and Animitsa, I., Double perovskites with oxygen structural vacancies: Raman spectra, conductivity and water uptake. *Solid State Ionics*, 2001, **145**, 339–347.
20. Dietrich, B. and Dombrowski, K. F., Experimental challenges of stress measurements with resonant micro-Raman spectroscopy. *J. Raman Spectr.*, 1999, **30**, 893–897.
21. Born, M. and Wolf, E., *Principles of Optics*. Pergamon Press, Oxford, 1985, p. 441.
22. Pezzotti, G., Sbaizero, O., Sergo, V., Muraki, N., Maruyama, K. and Nishida, T., In situ measurements of frictional bridging stresses in alumina using fluorescence spectroscopy. *J. Am. Ceram. Soc.*, 1998, **81**, 187–192.
23. Meggers, W. F. and Humphreys, C. J., *Bur. Stand. J. Res.*, 1934, **13**, 293.
24. Gibson, U. J. and Chernuschenko, M., Ruby films as surface temperature and pressure sensors. *Optics Express*, 1999, **4**, 443–448.
25. He, J. and Clarke, D. R., Determination of the piezospectroscopic coefficients for chromium-doped sapphire. *J. Am. Ceram. Soc.*, 1995, **78**, 1347–1353.
26. Jia, W. and Yen, W. M., Raman scattering from sapphire fibres. *J. Raman Spectr.*, 1989, **20**, 785–788.
27. Shin, S. H., Pollak, F. H. and Raccah, P. M., In *Proceedings of the Third International Conference on Light Scattering in Solids*, 1975, pp. 401–405.
28. Gallas, M. R., Chu, Y. C. and Piermarini, G. J., Calibration of the Raman effect in a-Al_2O_3 ceramic for residual stress measurements. *J. Mater. Res.*, 1996, **10**, 2817.
29. Jovanic, B. R. and Andreeta, J. P., Effects of high pressure on the fluorescence spectra of Cr^{3+} in $GdAlO_3$. *J. Phys.: Cond. Matter*, 1998, **10**, 271–274.